

# RSC Advances



This is an *Accepted Manuscript*, which has been through the Royal Society of Chemistry peer review process and has been accepted for publication.

*Accepted Manuscripts* are published online shortly after acceptance, before technical editing, formatting and proof reading. Using this free service, authors can make their results available to the community, in citable form, before we publish the edited article. This *Accepted Manuscript* will be replaced by the edited, formatted and paginated article as soon as this is available.

You can find more information about *Accepted Manuscripts* in the [Information for Authors](#).

Please note that technical editing may introduce minor changes to the text and/or graphics, which may alter content. The journal's standard [Terms & Conditions](#) and the [Ethical guidelines](#) still apply. In no event shall the Royal Society of Chemistry be held responsible for any errors or omissions in this *Accepted Manuscript* or any consequences arising from the use of any information it contains.

Cite this: DOI: 10.1039/c0xx00000x

www.rsc.org/xxxxxx

ARTICLE

## Electrospun BiOI nano/mesoporous tectonic plate like structures synthesis and UV light assisted photodegradation of ARS dye †

Veluru Jagadeesh Babu,<sup>a</sup> R S R Bhavatharini,<sup>b\*</sup> and Seeram Ramakrishna,<sup>\*b,c</sup><sup>5</sup> Received (in XXX, XXX) Xth XXXXXXXXX 20XX, Accepted Xth XXXXXXXXX 20XX

DOI: 10.1039/b000000x

BiOI electrospun nanofibers were prepared by using PAN as supporting polymer. The subsequent annealing at 500 °C for 5 h, with a ramp rate of about 5 °C/min in air, breaks down to tectonic plates like nano/micro structures. The surface physical and chemical structural changes were then further characterized by using FE-SEM, TEM, XRD and XPS. The results reveal that the morphology and crystallite size of BiOI vary strongly depending on the precursor concentration used in the synthesis method. These nano-structures were later employed for photocatalytic degradation of a synthetic textile dye, Alizarin Red S (ARS). The photocatalytic efficiencies were found to be about 93.34 % after 100 min of UV (340 nm) light illumination. Photocatalytic activity performance depends on morphology and band alignment. All the compositions follow the first order pseudo kinetics, which was found 0.1197 min<sup>-1</sup> for the 3% of doping concentration. The enhancement in photodegradation can be possibly by photocatalysis and photosensitization phenomenon, being explained based on the band edge position.

### Introduction

There has been an increased attention for the bismuth oxohalide (BiOX) materials, in environmental remediation applications<sup>1, 2</sup>. Especially, the low dimensional nano/micro structures<sup>3</sup>, show their influence on physical and chemical properties and thereby useful in tailoring (or) fine tuning of the electronic structures<sup>4, 5</sup>. They are part of the V-VI-VII ternary group semiconductors with the general formula, A<sup>V</sup><sub>m</sub> B<sup>VI</sup><sub>n</sub> X<sup>VII</sup><sub>p</sub> where [A = bismuth (Bi), arsenic (As), (or) antimony (Sb); B = oxides (O), sulphides (S), (or) selenides (Se) and X = halides such as Cl, Br, I] belonging to the tetragonal system<sup>6</sup>. The structure of bismuth oxohalides are known to have a layered, matlockite structure (PbFCl type structure with SG: P4/nmm). They contain a layer-like morphology with [Bi<sub>2</sub>O<sub>2</sub>]<sup>2+</sup> slabs found alternative with respect to double (halogen)<sup>-</sup> slabs, which yields a plate-like morphology<sup>7, 8</sup>.

Two types of binding forces were observed in these compounds—a strong intralayer bonding in [Bi<sub>2</sub>O<sub>2</sub>]<sup>2+</sup> and relatively weak Van der Waals forces between the layers like sandwich structures. The enhanced photocatalytic activity of the catalysts might be attributed to the efficient separation of the photogenerated electron-hole pairs caused by static internal electric forces between [Bi<sub>2</sub>O<sub>2</sub>]<sup>2+</sup> slabs and the anionic halogen layers<sup>9</sup>. This static internal force in turn can be controlled by carefully choosing the structure and morphology of the materials. Based on these binding forces, crystal morphology, structural anisotropy and synthesis routes, these bismuth oxohalides are proven to show several exotic properties (physical and chemical) such as electrical, magnetic, luminescent, mechanical, photocatalytic,

optical and photophysical properties (tunable emission wavelengths and enhanced fluorochrome quantum yields)<sup>10, 11</sup>.

Among these oxohalides, BiOI has been reported to be an efficient visible light driven photocatalyst utilized for the degradation of methyl orange, phenol and other well known organic pollutants<sup>12, 13</sup>. The band structures for BiOI, the valence band (VB) and conduction band (CB) at 2.39 eV, and 0.48 eV apart, respectively<sup>6</sup>. Hence the estimated band gap is about 1.91 eV, very strong absorption in visible light region and results in best performance of photocatalytic dye degradation. But, due to the quick recombination of the photoexcited charge carriers, the photocatalytic activity of the BiOI is limited<sup>14, 15</sup>. So, the photocatalytic reactivity of the BiOI must be further enhanced to be useful in practical applications. However for an effective photodegradation, it is imperative to discover a suitable and simple synthesizing technique that enables to control the morphology and thereby its influence on photocatalytic performance of BiOI.

The objective of this study, BiOI nanofibers were synthesized through the electrospinning that is a simple efficient technique used for the preparation of 1D-nanomaterials for its precise control of the diameter of the fibers thus produced. The electrospun nanofibers were annealed at 500 °C for 5 h, with a ramp rate of about 5 °C/min in air. After the heat treatment, the uniform and smooth electrospun nano structures break down into nanotectonic plate like structures due to the evaporation of the polymer content. The synthesized samples had undergone the XRD, microscopy, spectroscopy, and photocatalysis studies. The photocatalysis studies reveal that the nanotectonic plate like structures has shown to produce enhancement in

photodegradation towards Alizarin Red S (ARS) dye under UV-light irradiation.

## Experimental Section

### Materials

5 Bismuth (III) Iodide (99%), Poly Acrylo Nitrile (PAN, Mw = 150,000 Da), N,N-Dimethylformamide (DMF) (anhydrous 99.8%), and Alizarin Red S (ARS) were obtained from Sigma Aldrich Chemical Company, Inc., St. Louis, U.S. All chemicals were used without further purification.

### 10 Preparation

The fiber deposition parameters (flow rate, applied voltage, drum rotation speed, etc.) were optimized until uniform nanofibers without bead formation were obtained<sup>16, 17</sup>. For the preparation of BiOI nanofibers, PAN solution of about 10.0 wt. % was initially prepared by dissolving PAN powder in DMF and it was left for stirring about 2 hours. After a reasonably miscible solution was obtained, 1% of BiI<sub>3</sub> was then added to the as-prepared miscible solution of PAN, followed by vigorous stirring at room temperature for 12 h to form homogeneous yellowish solution.  
20 This process was then repeated to various concentrations of the BiI<sub>3</sub> (2%, 3% and 4% w/v) in PAN. The solution was taken in a 10 mL syringe with 21 G 1/2 gauge needle. The flow rate was maintained to 1.0 mL/h and the distance between the electrodes (tip of the needle to collector) was maintained at about 10 cm.  
25 The applied electric voltage between the drum collector and the tip of the needle was 20kV and the humidity level inside the electrospinning chamber was maintained<sup>18</sup> throughout the experiment at approximately 50%.

The as-spun material collected on the Aluminium foil was annealed at 500 °C for 5 h, with a ramp rate of about 5 °C/min in air. The uniform and continuous nanofibers break down into unique nanostructures (based on the used precursors)<sup>19, 20</sup> during the sintering process due to the decomposition of PAN. These electrospun nanofibers converted nanoplates were later vacuum-dried to remove any residual solvent.

### Characterization

The surface characterization was done using the Field Emission-Scanning Electron Microscope (FESEM; Quanta 200F, FEI, Oregon, U.S.) on the samples that were previously gold-coated (JEOL JFC-1200 fine coater, Japan). Transmission electron microscopy (TEM) was used to characterize the morphology of the synthesized particles and the TEM images were obtained on a JEOL JEM-2010F Transmission Electron Microscope, operated at an acceleration voltage of 200 kV. The crystal structures of the BiOI were characterized by using PANalytical X'Pert Pro multipurpose X-ray diffractometer (XRD) in the range of 2θ = 5–80° with intensity of CuKα (1.5418 Å) radiation for the high concentration. The elemental study was done by X-ray photoelectron spectra using Kratos AXIS Ultra DLD (Kratos Analytical Ltd., U.K.).

### Photocatalytic degradation

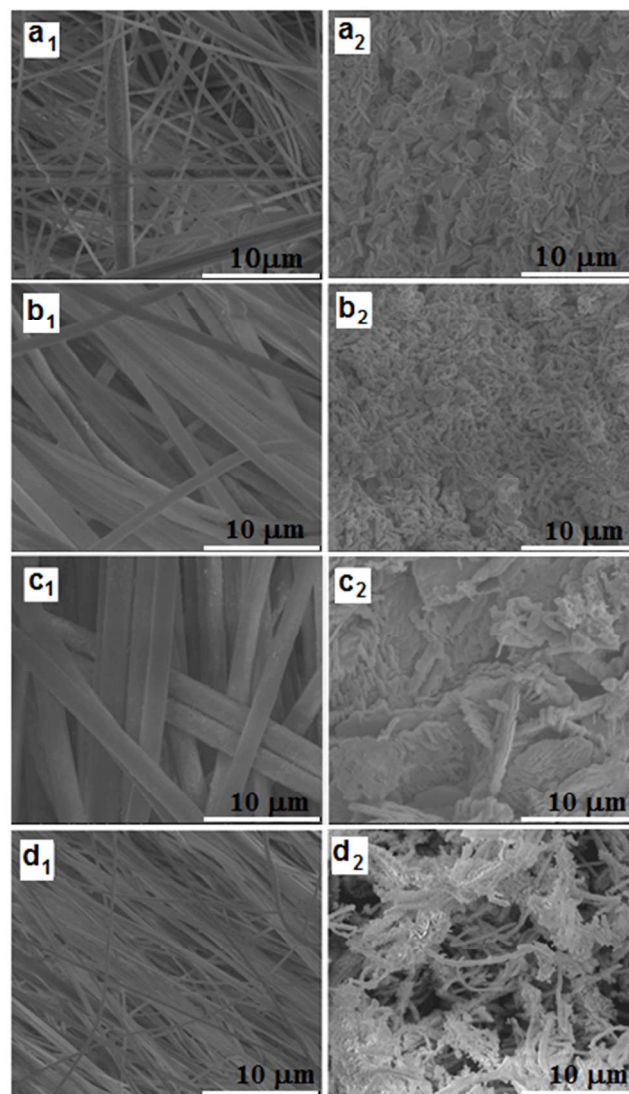
A suspension of the nanofibrous photocatalyst and an aqueous

ARS solution was prepared as reported previously<sup>19, 20</sup>. The dye solution was prepared by dissolving 50 mg of ARS powder in 50 mL of de-ionized (DI) water. The suspension was ultrasonicated for about 30 min to obtain a homogeneous solution and establish adsorption–desorption equilibrium between the organic molecules and the catalyst surface. Initial concentration ( $C_0$ ) of the dye is measured before being exposed to the UV-irradiation. Later the dispersion is placed in such a way that it is completely surrounded by the light source (a conventional UV lamp was used as the light source)<sup>19</sup>. Decreases in the concentrations of dyes were analyzed by a UV–Vis spectrophotometer, of model: Shimadzu UV3600 (spectral resolution of 1 nm). Then, at given intervals of illumination, the samples of the reaction solution were taken out and absorption spectra were analyzed.

## Results and Discussion

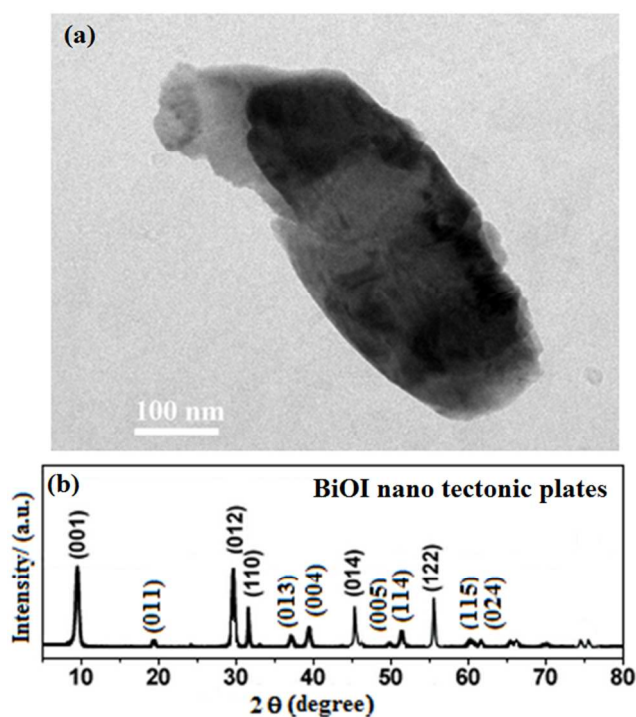
### Physico-Chemical Characterization

Figure 1 (a<sub>1</sub>, b<sub>1</sub>, c<sub>1</sub> and d<sub>1</sub>), shows the SEM images of the as-synthesized electrospun BiOI nanofiber mats at different blend compositions with a fixed total solution concentration of about 10 wt% PAN solution in DMF.



**Figure 1:** SEM images of  $a_1$ ,  $b_1$ ,  $c_1$  and  $d_1$  as-spun nanofibers and  $a_2$ ,  $b_2$ ,  $c_2$ , and  $d_2$  sintered BiOI at concentrations of 1, 2, 3, and 4 % (w/v).

To obtain smooth, bead-free nanofibers, this content needed to be maintained to 10%. At all considered blend compositions, the nanofibers were found to be uniform and aligned with slightly rough surfaces. At lower loadings the fibers seem to be uniform. But as increasing the concentration of the iodine, the fibers become uniform and more smoother. Fig. 1 ( $a_2$ ,  $b_2$ ,  $c_2$ , and  $d_2$ ) exhibits the SEM micrograph of BiOI that showed a different morphology with anomalous rough textured nanoplates, and the sizes of these rounded nano and microplates were less than 2  $\mu\text{m}$ , whose regular shapes suggest they are of crystalline nature. They intersect with each other over various orientations with the surrounded neighbouring nanoplates systematically forming a step-like feature as can be seen in fig.1 ( $b_2$  &  $c_2$ ). As shown in fig. 1 ( $c_2$ ), the overall FESEM images present a panoramic morphology of the dispersed nanoplates with thickness in the range of 400–800 nm, indicating that the high yield and uniformity of the BiOI “nanotechtions” like structures<sup>21</sup> can be prepared by this simple, facile route.



**Figure 2:** (a) TEM image of a single BiOI nanotechtion plate like structure, and (b) XRD patterns obtained on BiOI nanotechtion plates

High resolution TEM image of a single nano tectonic plate/rod shape is shown in figure 2 (a). The TEM image reveals that the BiOI tectonic plate is a well-defined longish particle with average size of ~150 to 200 nm, confirming the SEM revelations. Suggesting the BiOI tectonics is preferably best morphological structure for the photocatalytic reactions. The XRD pattern of nanotechtions is shown in figure 2 (b). From the XRD, all the peaks have been identified and perfectly indexed related to the BiOI and there are no other peaks for impurities. It reveals that the BiOI is high pure by the production method of electrospinning. The average crystalline sizes were been calculated from XRD, about ~168 nm at the (001) lattice plane by using the Scherer formula ( $d = 0.94\lambda / \beta \cos\theta$ )<sup>22, 23</sup>, where  $d$  is the

crystal size,  $\lambda$  is the wavelength of the  $\text{CuK}\alpha$  radiation,  $\beta$  is the FWHM in radians (full width at half maxima),  $\theta$  is the Bragg's angle for diffraction peaks.

X-ray Photoelectron Spectroscopy (XPS) of the BiOI nanostructures is provided in figure 3 (a). In Fig.3, Bi, O, I, and C elements could be seen. It can also be observed that the Spin Orbit Splitting (SOS) peaks of Bi 4f level is split into two peaks centred at 165.0 and 160.1 eV, which belong to the Bi 4f 5/2 and Bi 4f 7/2, respectively. By this, the main chemical states of Bi element in the samples proved tri-valent ( $\text{Bi}^{3+}$ ). The C 1s peak at 284.8 eV, can be attributed to the adventitious elemental carbon on the surface of the sample from experimental conditions. From the survey spectrum, the presence of O 1s peak showed the fitted peak near 530 eV, which was ascribed to the Bi–O bonds in BiOI<sup>23</sup>.

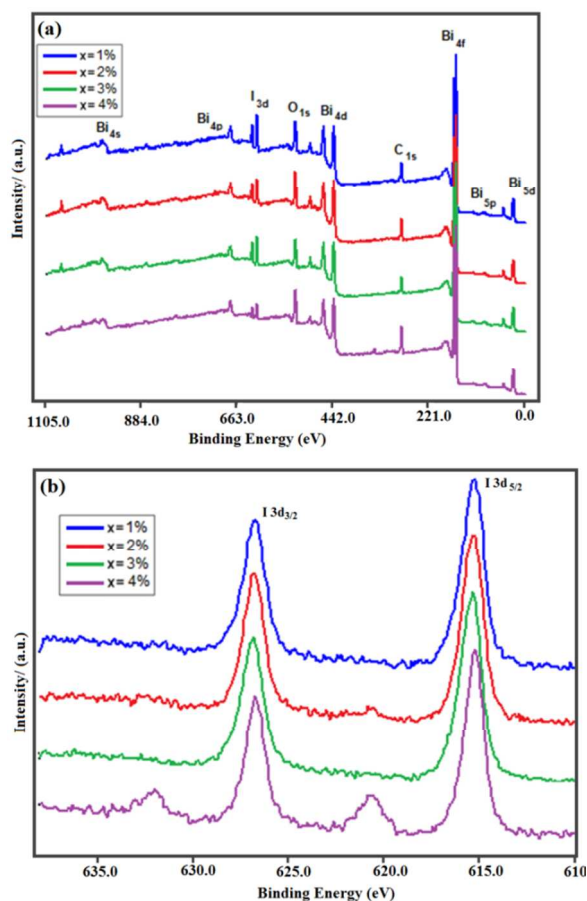


**Figure 3:**(a) XPS survey spectrum of the BiOI (b) High Resolution XPS I 3d spectrum at 1, 2, 3, and 4% (w/v).

For all the concentrations, there is only one dominating peak at 619.1eV. This shoulder may be due to  $\text{I}^{3-}$  doping of the polymers by iodine generated. The high-resolution I 3d<sub>5/2</sub> is shown in fig. 3(b). Two very strong peaks are observed at peak position 615.1 of I 3d<sub>5/2</sub> and another peak at 626.9 eV for I 3d<sub>3/2</sub> (fig.3(b)). These two peaks are the characteristic peaks of I within the BiOI. Thus it confirmed that all the levels of the doping. Only for the concentration 4%, there are two weak shorter peaks were observed at 620.6 and 631.7 eV, which may be attributed to the higher loadings of Iodine. From these short peaks, it can be

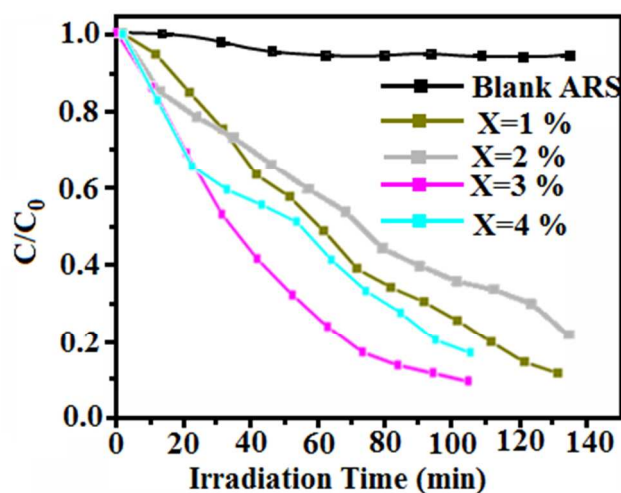
deduced that iodine atoms get attached via other atoms (probably carbon atoms) and not as pure iodine molecule.

## Photodegradation

The photocatalytic activity of the BiOI nanotechnic structures was characterized by degrading the quinine dye, ARS under UV-light irradiation at ambient temperatures<sup>19</sup>. The temporal evolution of the spectral changes during photodecomposition of ARS on the sintered BiOI samples under UV-light irradiation has shown in supporting information (SI 1<sup>†</sup>). A gradual degradation of the dye was observed, but near a wavelength of 240 nm, new peaks started to emerge, showing that there was an occurrence of new products. Photocatalysis studies on the dye without catalyst were very slow and almost nothing happened until 130 min. whereas, in presence of catalyst, the dye degraded considerable extent. However, the whole photocatalysis process of the ARS is extremely slow for concentrations at  $x=1$  and 2 %. This may be due to prolonged exposure of the photocatalyst in an aqueous solution, that led to the loss of surface Iodine, and which further proceeds to form an insulating bismuth hydroxide layer that prevents photochemical activity<sup>12</sup>. This might prove why there are new peaks in the 240 nm absorption spectrum and the photo-electrochemical instability of the bismuth oxyiodide in aqueous electrolytes. It has also been reported that semiconductor materials with small band-gap showed either low carrier mobility and absorption co-efficient<sup>24</sup>. Absorption peaks at 518 nm (shown in SI 1<sup>†</sup>), were used to monitor the photocatalysis process. The typical absorption peak gradually diminishes markedly with irradiation time and almost completely disappeared after 130 min (destruction of the complex structures)<sup>26, 27</sup>, suggesting good absorption and photocatalytic activities of the BiOI nano/micro techtonic plates. The photocatalysis of ARS is extremely slow without addition of catalysts and after addition of catalysts at only 3% of BiOI, the ARS degraded up to 93.34 % within 100 min under UV light irradiation. But at 4% of the BiOI samples executed limited photocatalytic performance under similar conditions, indicating that the adsorption equilibrium was reached at concentration level 3%. While, nearly 97% of ARS dye is degraded after 130 min (in case of 1% and 2% of the BiOI) over as prepared BiOI photocatalyst exhibits efficient photocatalytic activity under UV-light irradiation. Although, the lower concentrations of BiOI shows the efficient photocatalytic degradation for ARS, but in terms of photocatalytic efficiencies with respect to time will be poor. It was noteworthy that the structures at the concentration 4% shows the combination of nanofibers and nanoplates (can be seen from the fig 1 d<sub>2</sub>) are may not be distributed homogeneously throughout in ARS dye solution, only dispersion which is closely associated with light utilization and photocarrier transportation. Consequently, the absorption and photocatalytic activity of these structures cannot be more efficient. In comparison the nano/micro techtonic plates, combined structures (fibers and nanoplates in case of concentration 4%) belonging to the priority structure, have an unexpectedly (one can also see from the XPS, an abrupt peak at 621.3 eV) poorer absorption property for the ARS dye, which leads to a weaker catalyst effect (Fig. 4).

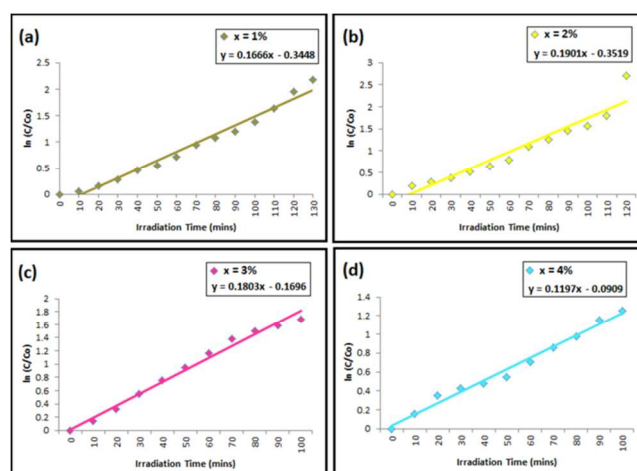
The nano/micro structures could provide more opportunities for the contact between light and contaminants, resulting in multiple

scattering of light. Actually, the photodegradation process is based on electron-hole pairs generated by band gap excitation and has no significant direct correlation with the specific surface area<sup>28</sup>. The effective separation of light-induced electrons and holes facilitates them to transfer to the surface to react with the absorbed reactants.



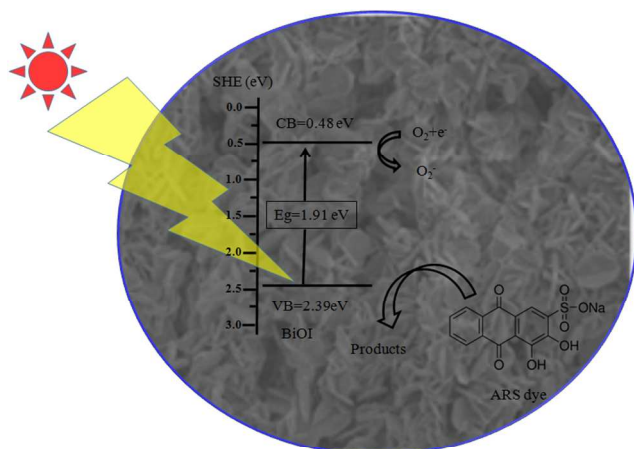
**Figure 4:** Photocatalytic reactivity of BiOI under UV-irradiation for blank ARS dye, concentrations at  $x=1, 2, 3,$  and  $4\%$  (w/v).

The corresponding ARS dye degradation graphs shown in figure 4. Figure 4 depicts the photodegradation of ARS without catalyst and with catalyst. It is observed that the aqueous solution with catalyst with different concentrations and ARS is effective under UV-illumination. There was no degradation observed for ARS after 130 min of UV irradiation, while for after adding the BiOI catalysts exhibits nearly 94% of the ARS dye degradation. Unique nanotechnic plate like structures are might be responsible for the excellent photocatalytic performance of the BiOI. ARS penetrated into the interlayer and high porous structures offer much more active sites accessible for photoreaction. The reactivity rates and photocatalytic efficiencies ( $\eta\%$ ) were obtained as 0.1124, 0.1850, 0.0666, and 0.2865  $\text{min}^{-1}$ ; 88.76, 81.49, 93.34, and 71.35 % for 1, 2, 3, and 4% respectively.



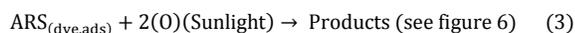
**Figure 5:** Kinetic plots and rate constant evaluation of BiOI photocatalyst at (a)  $x=1\%$ , (b)  $x=2\%$ , (c)  $x=3\%$  and (d)  $x=4\%$  (w/v).

The kinetics have been investigated on ARS dye degradation over the techtonic plates, and depicted in figure 5. The apparent first order kinetic equation was used to elaborate the experimental data<sup>29</sup>. The ARS dye degradation over BiOI was fitted well with first order kinetic equation. The graph plotted  $\ln(c/c_0)$  as a function of time ( $t$ ) displayed a straight line fit where  $c_0$  is the adsorption equilibrium concentration of ARS and  $c$  is the concentration of ARS at time ' $t$ '. The calculated kinetic rate constants  $k$  were 0.1666, 0.1803, 0.1901, and 0.1197  $\text{min}^{-1}$  for  $x=1\%$ , 2%, 3% and 4% correspondingly. The kinetic rate constant 'k' value is highest for the BiOI concentration at  $X=3\%$  when compared to other concentrations.



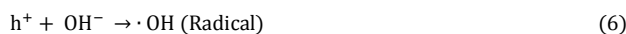
**Figure 6:** Schematic representation of the BiOI with dye degradation and band edge positions diagram.

Figure 6, clearly indicates the photodegradation mechanism in the ARS dye. Basically there are other two possible reaction mechanisms involved as photocatalysis<sup>30</sup> and photosensitization<sup>31</sup>. The photocatalysis: the pure ARS dye degradation without addition of any catalysts under light illumination with photon energy. The energy of photon could be transferred from the ARS dye to Oxygen, can act as oxidizing agent resulting photocatalysis for ARS dyes can be seen in Equations (1 to 3). From figure 4, one can also observe that the ARS dye could not degraded by photocatalysis without any added catalysts even after 130 min of irradiation, suggesting that ARS dye is stable.



The second one is the photosensitization: the pure ARS dye is adsorbed on the catalyst as sensitizer. The photo generated

electrons transfer from valence band (VB) to conduction band (CB), leaving holes behind VB top of the ARS dye. Then the excited electrons react with the oxygen to form oxygen radicals can be represented in equation (4 to 6). The generated oxygen radicals and holes can effectively oxidize the dye. The photosensitization equations presented from 7 to 10 equations<sup>23</sup>.



Hence, the photodegradation of ARS dye is initiated to undergo photocatalysis and photosensitization process together. The shown enhancement in the photodegradation is due to the fact that the electron-hole pairs generation, separation and transfer process. Eventually the photosensitization process is largely related to the surface properties and band alignment of the catalyst as shown in figure 6. VB and CB edge positions of the BiOI can be evolved from the following formulae (11 to 12)<sup>23, 32, 33</sup>.

$$E_{\text{VB}} = \chi_{(\text{semiconductor})} - E_{(\text{free electrons})} + 0.5 E_g \quad (11)$$

$$E_{\text{CB}} = E_{\text{VB}} - E_g \quad (12)$$

Where  $E_{\text{VB}}$  and  $E_{\text{CB}}$  are the VB and CB band edge potentials respectively,  $E_g$  is the band gap energy of semiconductor,  $\chi$  is the geometric mean of the electronegativity of the constituent atoms in a semiconductor.  $E$  is the energy of free electrons on the standard hydrogen energy (SHE:  $\sim 4.5$  eV). The evolved band edge positions for BiOI are 2.39 and 0.48 eV as VB and CB respectively.

## Conclusions

Rounded nano/micro-techtonic BiOI nanoplates have been synthesized by a controlled sintering of electrospinning parameters and precursors. By controlling the synthesis conditions, in this study, precursor concentration, facilitates us to tailor the diameters, morphology and thickness of BiOI platelets thus produced. The synthesized samples undergone for the XRD, microscopy, spectroscopy, and photocatalysis studies under UV-vis irradiation. The photocatalysis studies reveal that the nanotechtonic plate like structures produce a good photocatalytic activity towards Alizarin Red S under UV-light irradiation. However, ARS dye without adding catalyst (BiOI) exhibited a slow photodegradation under UV-light irradiation. The enhancement in photodegradation is may be due to effective generation, separation and transfer of electron and hole pairs. The estimated energy band edge positions and possible photodegradation processes have been formulated for BiOI

techtonic plates with the help of previous reports. Hence, the BiOI techtonic plates like structures are promising for high photocatalytic degradation of ARS dye.

## Acknowledgment

V J Babu, thanking The Scientific & Technological Research Council of Turkey (TUBITAK) (TUBITAK-BIDEB 2221, Fellowships for visiting scientists and scientists on sabbatical leave) for providing fellowship.

## Notes and references

<sup>a</sup> UNAM-National Nanotechnology Research Center, Bilkent University, Ankara, 06800 TURKEY.

E-mail: [babu@unam.bilkent.edu.tr](mailto:babu@unam.bilkent.edu.tr) (V J Babu),

<sup>b</sup> Center for Nanofibers and Nanotechnology, Nanoscience and Nanotechnology Initiative (NUSNNI), National University of Singapore, Singapore-117576,

<sup>c</sup> Department of Mechanical Engineering, National University of Singapore, Singapore-117576, Singapore.

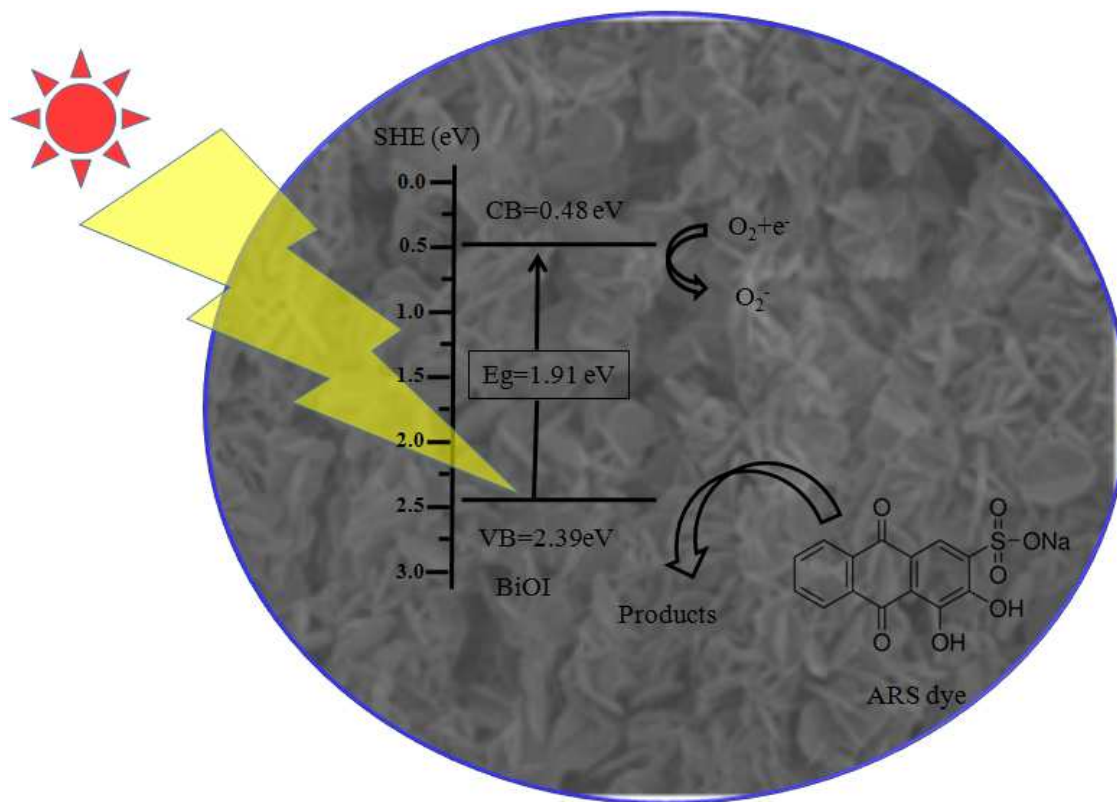
E-mail: [seeram@nus.edu.sg](mailto:seeram@nus.edu.sg) (S Ramakrishna).

† Electronic Supplementary Information (ESI) available: The photocatalysis studies on BiOI performed and shown in ESI 1.

See DOI: 10.1039/b000000x/

1. D. Chatterjee and S. Dasgupta, *J.Photochem.Photobiol. C*, 2005, 6, 186-205.
2. Y. Wang, K. Deng and L. Zhang, *J.Phys.Chem.C*, 2011, 115, 14300-14308.
3. V. J. Babu, S. Vempati, S. Sundarrajan, M. Sireesha and S. Ramakrishna, *Solar Energy*, 2013, DOI: <http://dx.doi.org/10.1016/j.solener.2013.1008.1037>.
4. D. L. Dhiman, V. S. Kundu, S. Arora and A. S. Maan, *AIP Conf.Proc.*, 2013, 1512, 598-599.
5. Y.-H. Lei and Z.-X. Chen, *J.Chem.Phys.*, 2013, 138, 054703.
6. X. Xiao, C. Liu, R. Hu, X. Zuo, J. Nan, L. Li and L. Wang, *J.Mater.Chem.*, 2012, 22, 22840.
7. T. B. Li, G. Chen, C. Zhou, Z. Y. Shen, R. C. Jin and J. X. Sun, *Dalton Trans*, 2011, 40, 6751-6758.
8. P. Kwolek and K. Szacilowski, *Electrochem.Acta*, 2012, DOI:10.1016/j.electacta.2012.1010.1001.
9. H. Zhang, L. Liu and Z. Zhou, *Phys.Chem.Chem.Phys.*, 2012, 14, 1286-1292.
10. L. Zhao, X. Zhang, C. Fan, Z. Liang and P. Han, *Physica B: Condensed Matter*, 2012, 407, 3364-3370.
11. H. Peng, C. K. Chan, S. Meister, X. F. Zhang and Y. Cui, *Chem.Mater.*, 2008, 21, 247-252.
12. N. T. Hahn, S. Hoang, J. L. Self and C. B. Mullins, *ACS Nano*, 2012, 6, 7712-7722.
13. Y. Li, H. Yao, J. Wang, N. Wang and Z. Li, *Mater.Res.Bullet*, 2011, 46, 292-296.
14. X. Zhang, Z. H. Ai, F. Jia and L. Z. Zhang, *J.Phys.Chem.C*, 2008, 112, 747.
15. X. Zhang, L. Z. Zhang, T. F. Xie and D. J. Wang, *J.Phys.Chem.C*, 2009, 113, 7371.
16. V. J. Babu, K. K. Satheesh, D. C. Trivedi, V. R. K. Murthy and T. S. Natarajan, *J.Engd.Fiber.Fabrics*, 2007, 2, 25-31.
17. V. J. Babu, V. S. P. Kumar, G. J. Subha, R. V. Kumari, T. S. Natarajan, A. S. Nair and S. Ramakrishna, *J.Engd.Fiber.Fabrics*, 2011, 6, 54-59.
18. V. J. Babu, R. P. Rao, A. S. Nair and S. Ramakrishna, *J.Appl.Phys*, 2011, 110, 064327.
19. V. J. Babu, A. S. Nair, Z. Peining and S. Ramakrishna, *Mater.Lett.*, 2011, 65, 3064-3068.
20. V. J. Babu, M. K. Kumar, A. S. Nair, T. L. Kheng, S. I. Allakhverdiev and S. Ramakrishna, *Int.J.Hydrogen Energy*, 2012, 37, 8897-8904.
21. Z. Bian, J. Zhu, J. Wang, S. Xiao, C. Nuckolls and H. Li, *J.Am.Chem.Soc*, 2012, 134, 2325-2331.
22. M. Galceran, M. C. Pujol, C. Zaldo, F. Díaz and M. Aguiló, *J.Phys.Chem.C*, 2009, 113, 15497-15506.
23. J. Cao, B. Xu, H. Lin, B. Luo and S. Chen, *Dalton Trans*, 2012, 41, 11482-11490.
24. K. Rajeshwar, *J.Appl.Electrochem.*, 1985, 15, 1-22.
25. Y. Bessekhouad and M. Trari, *Int.J.Hydrogen Energy*, 2002, 27, 357-362.
26. Y. Li, J. Wang, H. Yao, L. Dang and Z. Li, *J. Molecular Cat. A: Chemical* 2011, 334, 116-122.
27. K. Ren, K. Zhang, J. Liu, H. Luo, Y. Huang and X. Yu, *Cryst.Eng.Comm.*, 2012, 14, 4384-4390.
28. A. Rachel, M. Sarakha, M. Subrahmanyam and P. Boule, *Appl. Catal. B.*, 2002, 37, 293-300.
29. V. J. Babu, M. K. Kumar, R. Murugan, M. M. Khin, R. P. Rao, A. S. Nair and S. Ramakrishna, *Int.J.Hydrogen Energy*, 2013, 38, 4324-4333.
30. X. Lin, T. Huang, F. Huang, W. Wang and J. Shi, *J.Phys.Chem.B*, 2006, 110, 24629-24634.
31. C. Nasr, K. Vinodgopal, L. Fisher, S. Hotchandani, A. K. Chattopadhyay and P. V. Kamat, *J.Phys.Chem.B*, 2006, 110, 8436-8442.
32. Y. Li, J. Wang, H. Yao, L. Dang and Z. Li, *Catal.Commun.*, 2011, 12, 660-664.
33. Y. Xu and M. A. A. Schoonen, *American Mineralogist*, 2000, 85, 543-556.

## Graphical Abstract



BiOI electrospun techtonic plates like nano structures synthesized. The surface physical and chemical structural changes was then observed. Morphology and crystallite size of BiOI vary strongly depend on the precursor concentrations. These nano-structures were later employed for photocatalytic degradation of ARS dye. The photocatalytic efficiencies were found to be about 93.34 % after 100 min of UV (340 nm) light illumination. Photocatalytic activity performance depends on morphology and band alignment. All the compositions follows the first order psuodo kinetics, which is found  $0.1197 \text{ min}^{-1}$  for the 3% of doping concentration. The enhancement in photodegradation can be possibly by photocatalysis and photosensitization phenomenon, has been explained based on the band edge position.